Research Article | Vol. 9, No. 10 | 1 Oct 2018 | BIOMEDICAL OPTICS EXPRESS 4850
Biomedical Optics EXPRESS

Photodynamic opening of the blood-brain barrier to high weight molecules and liposomes through an optical clearing skull window

CHAO ZHANG,[1,2] WEI FENG,[1,2] ELENA VODOVOZOVA,[3] DARIA TRETIAKOVA,[3] IVAN BOLDYREVD,[3] YUSHA LI,[1,2] JURGEN KÜRTHS,[4,5,6] TINGTING YU,[1,2] OXANA SEMYACHKINA-GLUSHKOVSKAYA,[4,7,8] AND DAN ZHU[1,2,7,9]

[1]*Britton Chance Center for Biomedical Photonics, Wuhan National Laboratory for Optoelectronics-Huazhong University of Science and Technology, Wuhan, Hubei 430074, China*
[2]*MoE Key Laboratory for Biomedical Photonics, Collaborative Innovation Center for Biomedical Engineering, School of Engineering Sciences, Huazhong University of Science and Technology, Wuhan, Hubei 430074, China*
[3]*Shemyakin-Ovchinnikov Institute of Bioorganic Chemistry, Russian Academy of Sciences, Miklukho-Maklaya 16/10, Moscow 117997, Russia*
[4]*Saratov State University, Interdisciplinary Center of Critical Technologies in Medicine, Department of Physiology of Human and Animals, Astrakhanskaya Str. 83, Saratov 410012, Russia*
[5]*Humboldt University, Physics Department, Newtonstrasse 15, Berlin, Germany*
[6]*Potsdam Institute for Climate Impact Research, Telegrafenberg A31, Potsdam, Germany*
[7]*Co-corresponding authors*
[8]*glushkovskaya@mail.ru*
[9]*dawnzh@mail.hust.edu.cn*

Abstract: The photodynamic (PD) effect has been reported to be efficient for the opening of the blood-brain barrier (BBB), which provides a new informative platform for developing perspective strategies towards brain disease therapy and drug delivery. However, this method is usually performed via craniotomy due to high scattering of the turbid skull. In this work, we employed a newly-developed optical clearing skull window for investigating non-invasive PD-induced BBB opening to high weight molecules and 100-nm fluid-phase liposomes containing ganglioside GM1. The results demonstrated that the BBB permeability to the Evans blue albumin complex is related to laser doses. By *in vivo* two-photon imaging and *ex vivo* confocal imaging with specific markers of the BBB, we noticed PD-related extravasation of rhodamine-dextran and liposomes from the vessels into the brain parenchyma. The PD induced an increase in oxidative stress associated with mild hypoxia and changes in the expression of tight junction (CLND-5 and ZO-1) and adherens junction (VE-cadherin) proteins, which might be one of the mechanisms underlying the PD-related BBB opening for liposomes. Our experiments indicate that optical clearing skull window will be a promising tool for non-invasive PD-related BBB opening for high weight molecules and liposomes that provides a novel useful tool for brain drug delivery and treatment of brain diseases.

1. Introduction

The blood brain barrier (BBB) plays an important role in the central nervous system (CNS) health, which consists of the specialized endothelial cells, pericytes, basal lamina, and astrocytes [1]. This BBB complex controls penetration of blood-borne agents into the brain and protects the CNS from toxins and pathogens. However, it also limits delivery of therapeutics to CNS that poses a challenge for effectively therapy to majority of CNS diseases

#339938 https://doi.org/10.1364/BOE.9.004850
Journal © 2018 Received 17 Jul 2018; revised 16 Aug 2018; accepted 10 Sep 2018; published 14 Sep 2018

Biomedical Optics EXPRESS

[2]. Indeed, CNS diseases account for 30% of the total number in all diseases [3]. Therefore, the methods for opening of BBB have received significant attentions in the last decades [4–6]. There are a number of strategies have been attempted for overcoming BBB, including intracarotid arterial infusion of hyperosmolar solution [7]; focused ultrasound [8, 9]; intranasal delivery [10]; intrathecal & intraventricular delivery [11] and chemical disruption of BBB [12]. Nevertheless, these methods are not applicable in the clinical practice due to limitations such as invasiveness, limited parenchymal drug concentration, short opening period, low efficiency, occurrence of vasogenic edema etc [13, 14].

Recently, it has been revealed that PD, as a widely used tool for fluorescent resection of glioma [15, 16], can also effectively and site-specifically open BBB [17, 18]. PD is realized by combining light irradiation with photosensitizing agents (porphyrins, chlorins and many other photodynamic dyes). The excited photosensitizer directly oxidizes biomolecules and/or interacts with molecular triplet oxygen ($^3O_2$) producing singlet oxygen ($^1O_2$) that causes cancer cells apoptosis and/or necrosis through plasma and mitochondria membrane disrupture. 5-aminole-vulinic acid (5-ALA) is a pro-drug of photosensitizer that has been widely used in a variety of PDT applications due to its safety and suitability for oral administration [16]. After being administrated, 5-ALA is metabolized to protoporphyrin IX, exhibiting a photodynamic effect via light irradiation to the targeted tissue [16]. Typically, PD will induce the edema, which happens at the region surrounding the site of light treatment, suggesting a local degradation of the BBB [17–20]. Therefore, PD appears to have a two-fold effect: a direct antineoplastic effect on the remaining tumor cells as well as an effect that causes localized opening of the BBB [18]. Indeed, several publications demonstrate PD-mediated opening of BBB for both high and low weight molecules, such as the Evans Blue albumin complex 68.5 kDa, FITC-dextran 70 kDa, gadolinium 552 Da, as well for macrophages. However, the high scattering property of skull strongly limits light penetration. Therefore, craniotomy needs to be implemented before applying PD [17, 19]. But it will unavoidably induce the changes in intracranial pressure and cortical inflammation, which may cause some misinterpretations of mechanisms underlying PD-related BBB opening [21]. Madsen demonstrated the BBB opening through the intact skull but with high doses of photosensitizer and laser irradiation, which is often accompanied by severe vasogenic edema [18, 20].

Fortunately, optical clearing skull windows have been developed by topical treatment of chemical agents on skull to reduce the skull scattering [22–26]. They not only allow us to visualize cortical vasculature, neurons and microglia, but also permit to realize light manipulation to cortex, such as laser-induced neuron and microglia damages. Therefore, the optical clearing skull windows provide a potential way to open BBB by PD without craniotomy.

In this study, we investigated the efficiency of PD-related opening of BBB and the optimal laser dose through the optical clearing skull window. To evaluate the applicable significance of PD-induced BBB opening, we performed *ex vivo* and *in vivo* studies of BBB permeability to the Evans Blue albumin complex (68.5 kDa), rhodamine-dextran (70 kDa) and GM1-liposomes (100 nm), which act as good candidates for brain drug delivery systems. For better understanding the mechanisms responsible for liposomes penetration through BBB, we studied changes in the expression of molecular factors that regulating BBB penetration and in the indicators of oxidative stress such as the level of malondialdehyde in brain tissues as well the blood oxygen saturation (SpO_2) [27–29].

2. Materials and methods

2.1 Subject

The experiments were performed on 8-week-old male BALB/c mice in following groups: (1) control – without laser irradiation; (2) 5-ALA injection without laser irradiation; (3) laser irradiation without 5-ALA injection; (4) PD through the intact skull without optical clearing

Biomedical Optics EXPRESS

window; (5) PD through the intact skull after the treatment of skull optical clearing agent. The fourth and fifth groups were divided into 4 sub-groups corresponding to different laser doses: (4-1) (5-1) 10 J/cm^2; (4-2) (5-2) 20 J/cm^2; (4-3) (5-3) 30 J/cm^2; (4-4) (5-4) 40 J/cm^2. Each group and sub-group included 6 mice. All experimental procedures were performed according to animal experiment guidelines of the Experimental Animal Management Ordinance of Hubei Province, P. R. China, and the guidelines from the Huazhong University of Science and Technology, which have been approved by the Institutional Animal Ethics Committee of Huazhong University of Science and Technology.

2.2 Preparation of skull optical clearing agents

In our recent work, we have reported newly-developed skull optical clearing agents that can make the mouse skull transparent within 15 min, named USOCA [26]. USOCA consists of S1 and S2. S1 is a saturated supernatant solution of 75% (vol/vol) ethanol (Sinopharm, China) and urea (Sinopharm, China) at 25 °C. For preparing S1, ethanol is slowly dropped into and mixed with urea. The mixture is stirred constantly, then stands for 15 min to let the urea fully dissolve, after which the supernatant is obtained. The volume-mass ratio of ethanol and urea is about 10:3. S2 is a high-concentration sodium dodecylbenzenesulfonate (SDBS) solution that is prepared by mixing 0.7 M NaOH solution (Aladdin, China) with dodecylbenzenesulfonic acid (DDBSA, Aladdin) at a volume-mass ratio of 24:5, and the pH is 7.2-8. Both S1 and S2 should be stored at ~25 °C. The detailed application method of USOCA is reported in the reference [26].

2.3 PD-induced BBB opening through an optical clearing skull window

The mice were anesthetized with a cocktail of 2% α-chloralose and 10% urethane (8 mg/kg, iv) via intraperitoneal injection. The scalp was removed and the skull surface was dried by clean compressed air. Afterward, USOCA were used to establish an optical clearing skull window (diameter = 5mm) [26]. PD was performed in 30 min after intravenous injection of 5-ALA. We used 5-ALA with the clinically recommended dose (20mg/kg) [16]. A 635 nm laser (NJL-LD-635-5-F-R, China, bandwidth: 30 nm) was used to irradiate the mouse brain through optical clearing skull window. By adjusting the irradiation duration, we treated the mouse brain with different light doses at 10, 20, 30, 40 J/cm^2, respectively. The constant power fluence was 165 mW/cm^2 and the corresponding irradiation durations were 1, 2, 3 and 4 min, respectively. Figure 1 illustrates the schematic diagram of PD-related effects on the BBB through optical clearing skull window.

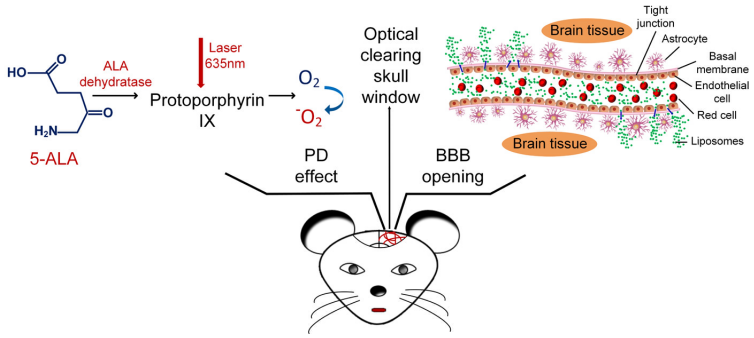

Fig. 1. PD-induced opening of BBB through optical clearing skull window

2.4 The preparation of GM1-liposomes

Liposomes have phospholipid bilayer structure (similar to physiological membrane) that makes them more compatible than other nanoparticles with the lipoidal layer of the BBB and helps the drug to enter the brain tissue [27, 29–34]. And they also display strong anti-glioma

Biomedical Optics EXPRESS

efficiency in *in vitro* and *in vivo* experiments, representing a promising platform for glioma therapy.

In this work, fluorescently-labelled GM1-liposomes were constructed on the basis of a matrix of egg yolk phosphatidylcholine (Lipoid GmbH, Germany) with a content of 10 mol.% ganglioside GM1 from bovine brain (Sigma Chemical Co., St. Louis, MO, USA) using a standard extrusion method [29]. Liposomes contained 1 mol.% BODIPY-phosphatidylcholine in the bilayer (λ_{ex} = 497 nm, λ_{em} = 504 nm) [34,35]. After hydration in physiological saline (phosphate buffer, pH 7.1, total lipid concentration 25 mM), the lipid film was subjected to seven cycles of freezing/thawing (liquid nitrogen/+40°C), and extruded 10 times through polycarbonate membrane filters (Nucleopore, USA) with a 100 nm pore diameter using Extruder Lipex (Northern Lipids, Canada). Colorimetric assay of the phospholipid concentration in liposome dispersion showed almost complete recovery of the material [36]. Particle size was assessed by dynamic light scattering using a 90Plus equipment (Brookhaven Instruments Corp., USA) in at least three runs per sample. Average size of liposomes was 87.2 ± 1.0 nm; PDI, 0.067. For reliable measurements of zeta potential, liposome samples were prepared as described earlier [37]. Briefly, lipid films hydrated in 10 mM KCl, 1 mM KH_2PO_4, 1mM K_2HPO_4 solution (pH 7.4), were subjected to freezing–thawing procedure followed by 20-fold extrusion through polycarbonate membrane filters with a pore size of 200 nm to gain liposome diameter at 200 nm. Zeta potential values were obtained using ZetaPALS analyzer (Brookhaven Instruments Corp., Holtsville, NY; provided by the CoreFacility of the Institute of Gene Biology, Russian Academy of Sciences). Samples of liposomes (1.5 ml, 1mg/ml total lipids) were equilibrated for 1 min in cuvettes before 10 runs of 25 cycles per sample, which was performed at 25°C. Two independent batches of liposomes showed an average zeta potential value of – 48.3 ± 0.9 mV (according to calculations using Smoluchowski approximation).

2.5 Assessment of the BBB permeability for high weight molecules and liposomes

For *ex vivo* evaluating BBB permeability, we tested Evans Blue dye (EBd) extravasation using a spectrofluorometric assay. After establishing optical clearing skull window, we performed PD. One hour after PD, EBd (Sigma Chemical Co., St. Louis, MI, USA) was injected in a single bolus dose (2 mg/25 g mouse, 1% solution in physiological 0.9% saline) through the tail vein. About 30 min after circulation, mice were decapitated, and their brains were rapidly taken out and placed on ice. The EBd extraction and measurement was performed accordingly to Wang et al [38].

For *in vivo* imaging of BBB permeability, we used two-photon laser scanning microscopy (2PLSM) to image the extravasation of rhodamine-dextran (70 kDa). Briefly, we established an optical clearing skull window on mice and intravenously injected rhodamine-dextran (Sigma, 4 mg/25 g) and let it circulated for 20 min. The cerebral vessels before PD were imaged by 2PLSM (A1R MP, Nikon, Japan) through optical clearing skull window. Then mice were intravenously injected 5-ALA (20 mg/kg) and in 30 min after circulation, PD was performed. Afterward, the same area of the brain was imaged again.

To investigate the efficiency of PD-related BBB opening for liposomes, we used three different markers to reveal the BBB integrity: 1) the endothelial barrier antigen conjugated with antibodies SMI-71 as a marker of cerebrovascular endothelium; 2) the anti-glial fibrillary acidic protein (GFAP) labelling astrocytes; and 3) the laminin, labelling the basal membranes.

In brief, liposomes were injected intravenously (0.2 ml/100 g, i.v.). 20 min after circulation, mice were decapitated and their brains were taken out rapidly and post-fixed in 4% paraformaldehyde (PFA, Sigma) for 24 hrs. After that, the brains were sliced into 100-μm on the vibratome (Leica VT 1000S Microsystem, Germany). The brain slices were permeabilized with PBST (1% PBS containing 0.2% Triton-X-100 (Sigma)) for 30 min, then we used 5% bovine serum albumin (BSA, Sigma) that dissolved in PBST to block the

Biomedical Optics EXPRESS

potential nonspecific binding sites for 45 min at room temperature. After that, the slices were immersed into the primary antibody (SMI-71: 1:200; GFAP: 1:200; laminin: 1:40) at 4°C overnight. Next, the slices were washed and incubated with the second antibodies (1:500) for 1 h at 25°C. Finally, the slices were imaged by confocal microscope (A1R, Nikon, Japan).

2.6 Immunohistochemical assay

Animals (8 weeks male Balb/c mice, 20-25 g) in the control group (before PD, n = 10) and experimental groups (1h, 24h and 72 h after PD, n = 10 in each group) were anesthetized, then intracardially perfused with PBS followed by 4% PFA, and brains were removed and sliced into 50μm.

The expression of antigens on free-floating sections was evaluated using the standard method of simultaneous combined staining (Abcam Protocol). Brain slices were blocked in 150 μl 10% BSA/0.2% Triton X-100/PBS for 2 h, then incubated overnight at 4°C with Rb anti-mouse Anti-beta Arrestin 1 antibody (1:500; Abcam, ab32099, Cambridge, USA); CLND-5 (1:500; Santa Cruz Biotechnology, sc-28670, Santa Cruz, USA); ZO-1 (1:500; Santa Cruz Biotechnology, sc-8147, Santa Cruz, USA); VE-cadherin (1:500; Santa Cruz Biotechnology, sc-6458, Santa Cruz, USA). After several rinses in PBS, the slices were incubated for 3 h at 25°C with fluorescently-labelled secondary antibodies in 1% BSA/0.2% Triton X-100 /PBS (1:500; Goat A/Rb, Alexa 555- Abcam, UK, ab150078). Following, the mice cerebral cortex was imaged using a fully automatic confocal laser scanning microscope (FV10i-W, Olympus, Japan). ImageJ was used for image data processing and analysis. The areas of expression of antigens were calculated using plugin "Analyze Particles" in the "Analyze" tab, which calculated the total area of antigen-expressing tissue elements - the indicator "Total Area". In all cases, 10 regions of interest were analyzed.

2.7 Histological analysis of the brain tissues

To assessment the changes of the brain tissues after PD, mice were decapitated after performing experiments for morphological analysis. The brain samples were fixed in 4% PFA for 24 hrs and then embedded in paraffin. After that, the brains were sectioned (4 μm) and stained with haematoxylin/eosin, then analysed using microscope (Nikon, Japan).

2.8 Malondialdehyde (MDA) analysis

The collected tissue samples were rinsed with saline solution, blotted and preserved at −196°C before the MDA assay performed. Before the test started, tissue was homogenized in 0.1 mol/L phosphate-buffer (pH 7.4) at 4°C using homogenizer (ULIRA-TURRAXT18, VWR, USA). The homogenates were then centrifuged at 4000 rpm for 10 min. The supernatants were collected and used for MDA analysis. MDA level was measured according to the methods described before [39].

2.9 Measurement of the blood oxygen saturation (SpO_2) in the brain

Level of SpO_2 in the brain, as an important criterion of cerebral metabolic activity, was monitored using pulse oximeter model CMS60D (Contec Medical Systems Co., Ltd., Qinhuangdao, China). Optical sensor was based on dual wavelengths pulse oximetry approach, using 660 nm and 880 nm for the SpO_2 detection. The SpO_2 is given as a percentage of HbO_2 vs. the total Hb in the blood as presented in our previous publication [40].

2.10 Statistical analysis

All data are expressed as mean ± standard error unless stated otherwise. Significant differences were analysed using one-way analysis of variance test with SPSS (IBM, USA).

Biomedical Optics EXPRESS

3. Results and discussion

3.1 PD-induced BBB opening for the EBd albumin complex: ex vivo data

At the first step, we analyzed laser-dose dependent PD effects on BBB permeability using spectrofluorimetric assay of EBd content in the mouse brain [36, 38]. EBd, a 961 Da dye that binds to serum albumin, becoming a high molecular weight complex (68.5 kDa) in the blood, which cannot pass through intact BBB. Thus, EBd leakage is an indicator of BBB disruption.

We used 165 mW/cm^2 laser irradiation, and the duration were 1, 2, 3 and 4 min, respectively. Thus, the corresponding laser doses were 10, 20, 30 and 40 J/ cm^2, respectively.

Our results in Table 1 indicated that there were no changes in BBB permeability to the EBd albumin complex in untreated mice and mice that only received 5-ALA injection or laser with different doses. The similar results were found in mice underwent PD (5-ALA + laser) without skull optical clearing treatment. However, PD with usage of USOCA accompanied by high concentration of EBd in the brain, suggesting strong EBd leakage through opened BBB. The comparison between groups of mice underwent PD with and without USOCA showed that laser dose of 10 J/ cm^2 caused an 10.3 fold increase of EBd leakage, 20 J/ cm^2 – an 20.2 fold; 30 J/ cm^2 – an 22.3 fold; 40 J/ cm^2 – an 22.9 fold.

Table 1. PD-induced BBB opening for the EBd albumin complex

Groups	Content of Evans Blue in the brain (μg/g tissue)			
Untreated mice	0.685 ± 0.012			
5-ALA	0.650 ± 0.011			
Laser 10, 20, 30, 40 J/cm^2	0.708 ± 0.007	0.673 ± 0.003	0.700 ± 0.006	0.801 ± 0.011
PD (5-ALA + laser) without optical clearing skull window				
10, 20, 30, 40 J/cm^2	0.741 ± 0.017	0.687 ± 0.013	0.807 ± 0.015	0.796 ± 0.010
PD (5-ALA + laser) with optical clearing skull window				
10, 20, 30, 40 J/cm^2	7.618 ± 0.496 ***	13.863 ± 0.712 ***	18.017 ± 1.171 ***	18.295 ± 1.466 ***

***-p<0.001 the comparison between untreated mice and mice underwent PD through optical clearing skull window, n = 6 in each group and sub-group.

The occurrence of vasogenic edema after PD therapy (PDT) is the main complication of this procedure due to direct laser effect on the brain tissues and intracranial pressure increase after craniotomy [19]. To find the optimal PD effects on BBB permeability with the appropriate vascular leakage but minimal brain injuries, we next analyzed morphological changes in the brain tissues and cerebral vessels after application of PD with different laser doses. As shown in Fig. 2, PD-related BBB opening was accompanied by vasogenic edema (pointed by black arrows) that was described also in our previous work [19]. The low laser doses (10 J/cm^2 and 20 J/cm^2) caused mild accumulation of solutes around microvessels, while higher laser doses (30 J/cm^2 and 40 J/cm^2) induced stronger vasogenic edema.

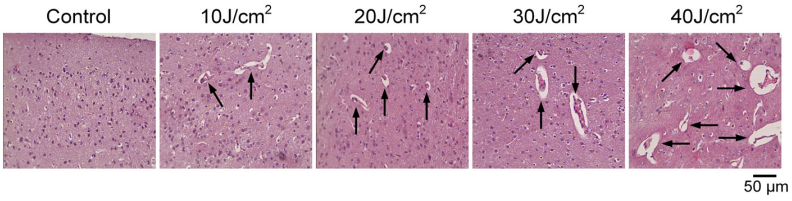

Fig. 2. The histological analysis of PD-related changes in the brain tissues and cerebral vessels. The black arrows show vasogenic edema.

Thus, low laser doses of 10 and 20 J/cm^2 caused less pathological changes in the brain vessels and tissues than high laser doses of 30 and 40 J/cm^2, which also have been shown in other works [19]. The further observation showed different time for recovering of the brain

Biomedical Optics EXPRESS

tissues after PD: in 72 hours with low laser doses of 10 J/cm^2 and 20 J/cm^2 and in 10-18 days with high laser doses of 30 and 40 J/cm^2 [18, 19].

Considering the fact that the EBd leakage was more pronounced with laser dose of 20 J/cm^2 vs. 10 J/cm^2 but comparable morphological changes in the brain tissues, we used 20 J/cm^2 in other experiments as optimal PD effect on the BBB.

3.2 PD-induced BBB opening for rhodamine-dextran: in vivo data

In this experimental set, we *in vivo* studied PD (20 J/cm^2)-induced BBB opening and imaged by 2PLSM through optical clearing skull window.

Figure 3 demonstrates PD-related opening of the BBB for rhodamine-dextran, which was determined by quantitatively measuring fluorescence signal intensity inside and around the cerebral vessels. Figure 3(a) is the timeline of the experiment. Firstly, 5- ALA (20mg/kg) was intravenously injected into the anaesthetic mice and circulated for 30 min, in this duration, the optical clearing skull window was established by topical application of USOCA. Then we imaged the cerebral vessels through the optical clearing skull window using 2PLSM. After that, 635 nm laser was applied to irradiate the mouse brain through the window, with the constant power fluence at 165 mW/cm^2 and 2 min irradiation durations. 1 h after laser irradiation (BBB was opened), we imaged the cerebral vessels at the same region again. We randomly selected 6 corresponding areas for quantitative analysis of signal intensity before and after PD (Fig. 3(d) and (e)). 1 hour after PD, we observed strong leakage of rhodamine-dextran (70 kDa) from the cerebral vessels into perivascular space resulting in the high fluorescent signal around the cerebral microvessels. Indeed, fluorescent signal in perivascular space increased 2.0-fold, suggesting high leakage of rhodamine-dextran from the cerebral vessels into the brain parenchyma via the opened BBB. The fluorescent signal in the cerebral vessels decreased 2.3-fold due to rhodamine extravasation into the brain tissues, metabolism by kidney, and even probably some photobleaching [41, 42] (Fig. 3(f)).

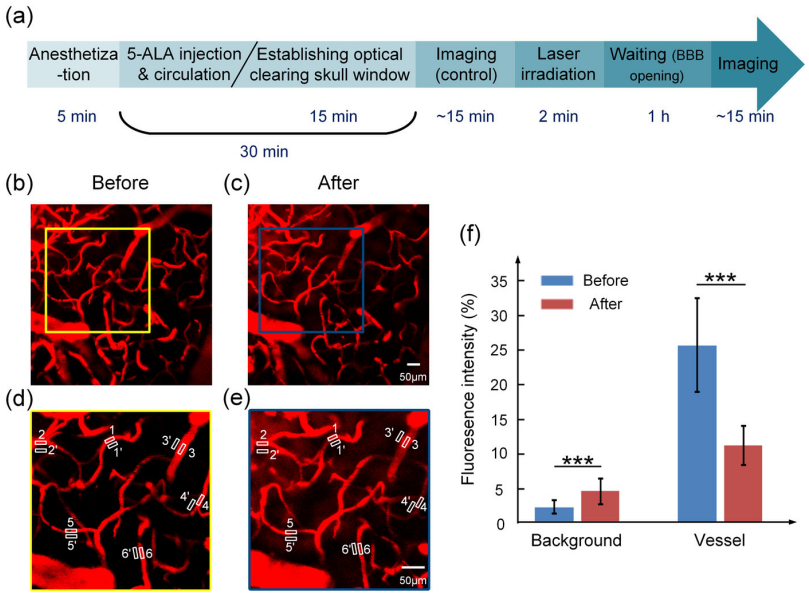

Fig. 3. The *in vivo* analysis of PD-induced BBB opening for rhodamine-dextran. (a) The timeline of the experiment. (b) and (c) are the same area imaged by 2PLSM before and after PD. (d) and (e) are the magnified images corresponding to the areas boxed in (b) and (c), respectively. (f) The bar graph of the average signal intensity inside (1-6) and outside (1'-6') vessels.

Biomedical Optics EXPRESS

These series of *in vivo* experiments confirmed our *ex vivo* data, suggesting non-invasive PD-related BBB opening for high weight molecules with the assistance of optical clearing skull window.

3.3 PD-induced BBB opening for GM1-liposomes

As a clinical applicable aspect of our work, we studied the effectiveness of PD-related BBB opening for liposomes as promising nanocarriers for brain drug delivery and anti-glioma therapy [27–33].

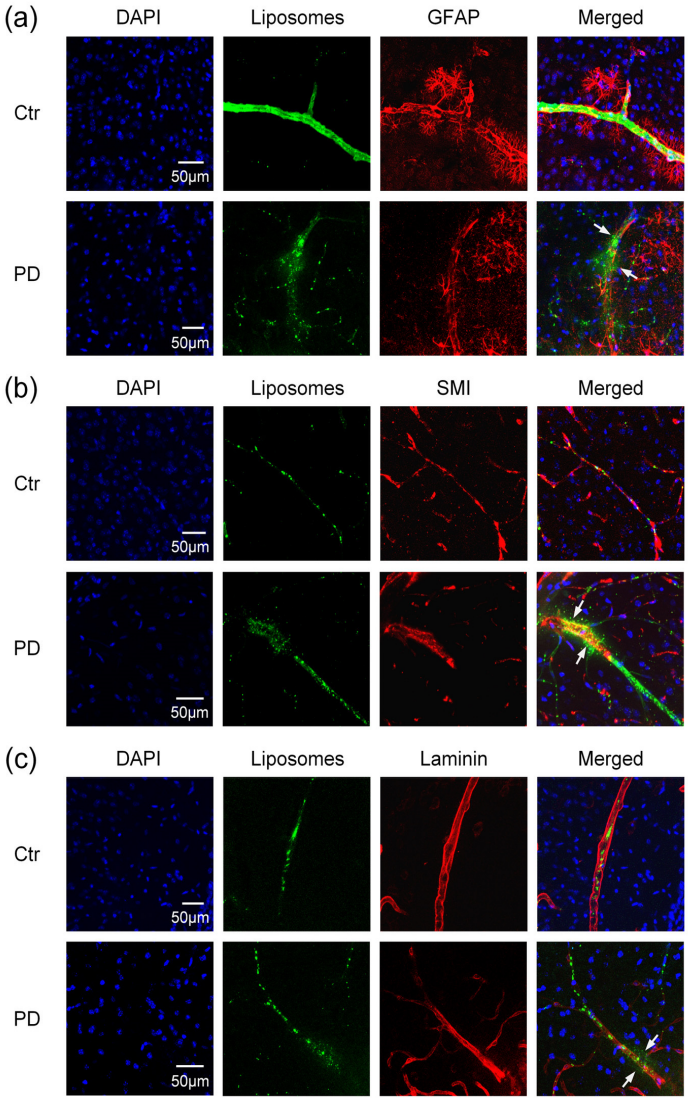

Fig. 4. The confocal imaging of non-invasive PD-induced BBB opening for GM1-liposomes with usage of markers of neurovascular unit: (a) liposomes distributions between the astrocytes labelled by antibodies of GFAP; (b) liposomes leakage outside the vascular endothelial cells labelled by antibodies of SMI; (c) liposomes distributions outside the basal membrane labelled by antibodies of laminin. Approximately 10-12 brain slices per animal (n = 6) were imaged. The white arrows show the sites of liposomes leakage.

Here, we analyzed BBB permeability to GM1-liposomes (100 nm) and investigated neurovascular unit integrity by using confocal microscopy. We have chosen such liposomes

Biomedical Optics EXPRESS

because GM1 was shown to contribute to both the stability of liposomes in the circulation to carry them to the brain [43] and their transport across BBB [33]. To study whether liposomes can cross BBB, we used markers of endothelial cell –SMI-71, the basal membrane – laminin, astrocytes endfeet – GFAP.

Figure 4 demonstrates effective extravasation of liposomes from the cerebral vessels into the brain parenchyma via opened BBB. We observed distribution of liposomes among the astrocytes (Fig. 4(a)) and outside of the cerebrovascular endothelium and the basal membrane (Fig. 4(b) and (c)).

Collectively, our results markedly show non-invasive PD-related opening of BBB for GM1-liposomes (100 nm) and their effective extravasation thought all elements of BBB including the vascular endothelium, the basal membrane and the astrocyte feet.

3.4 Mechanisms underlying the PD-induced opening of the BBB

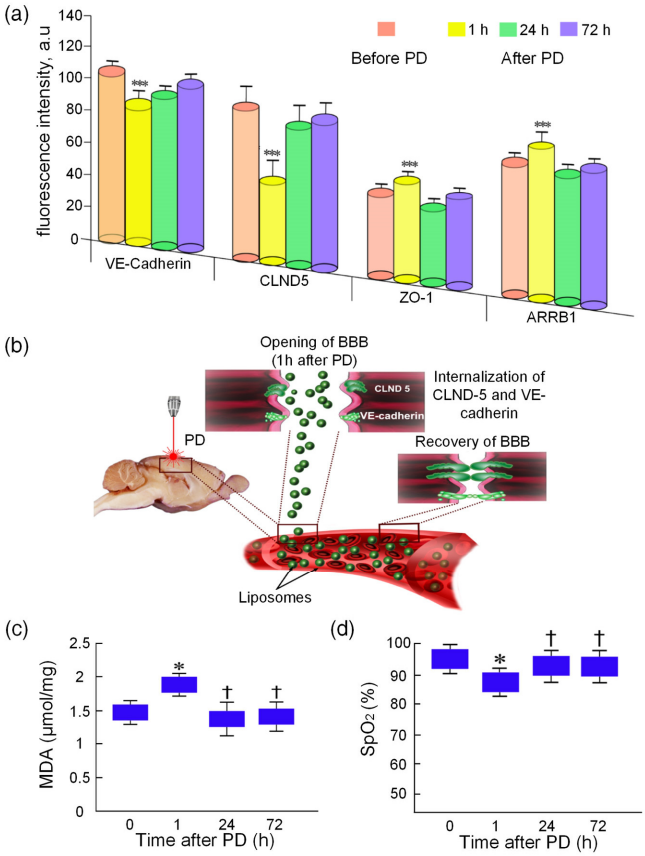

Fig. 5. Mechanisms underlying PD opening of BBB for GM1-liposomes. (a) The expression of TJ (CLDN-5 and ZO-1) and adhesion (VE-cadherin) proteins as well trans-membrane protein of cellular signalling system (ARRB1). ***-$p<0.001$, the comparison between PD-treated mice and untreated mice. (b) Schema of photodynamic opening of BBB: PD activates the internalization of CLND-5 and VE-cadherin that is accompanied by the loss of surface of these proteins in the space between vascular endothelial cells. (c) The PD-induced changes in the MDA level in the brain tissues. (d) The PD-induced changes in cerebral SpO_2. *-$p<0.05$ the comparison between PD-treated mice and untreated mice.

To better understand mechanisms responsible for PD-induced opening of BBB for GM1-liposomes, we studied PD-related changes in the expression of molecular factors, which are involved in the control of BBB permeability such as tight junction (TJ) trans-membrane

Biomedical Optics EXPRESS

proteins (CLND-5 and ZO-1) and adherens junction protein (VE-cadherin), as well as molecular membrane factor (beta-arrestin-1, ARRB1) controlling expression of these complexes of BBB proteins. The expression of indicated molecular factors was analyzed before PD (the control group), 1h after PD (when BBB was opened) and 24h and 72h after PD (when BBB was closed and completely recovered).

Figure 5(a) demonstrates that BBB opening (1h after PD) was accompanied by decreases in expression of CLND-5 and VE-cadherin but increases in expression of ZO-1 and ARRB-1 compared with the control group. Important note that expression of indicated molecular factors almost recovered 24h after PD effects and persisted at the normal level 72h after PD application.

To study metabolic changes related to PD-induced opening of BBB, we analyzed the MDA level of brain tissues as a marker of oxidative stress and component of reactive oxygen species production, as well the SpO_2 in the brain, as an important criterion of cerebral metabolic activity [44]. Our results revealed that PD-mediated BBB opening was associated with the increase in MDA by 12% ($p<0.05$) and a decrease in SpO_2 by 10% ($p<0.05$) 1 h after PD effect (Fig. 5(b) and (c)).

Our results uncovered the elevated expression of ARRB1 that is marshal in signaling trans-membrane processes, and decreases in the expression of CLND-5 and VE-cadherin as main components of BBB integrity [45–47]. We assume that the ARRB1 induced the internalization of CLND-5 and VE-cadherin, accompanied by the loss of surface on these proteins in space between endothelial cells, which can be one of the mechanisms underlying PD-induced opening of BBB for liposomes. Our hypothesis is based on the results of other experiment demonstrating the mechanism of BBB disruption via ARRB2-mediated internalization of VE-cadherin induced by vascular endothelial growth factor (VEGF). The elevated expression of ZO-1 during PD-mediated opening of BBB on the background of lowered expression of CLDN-5 and VE-cadherin could also suggest disordered interactions of TJ proteins [48]. Our results are consistent with data of other research showing that PD has a direct effect on increasing the gaps of the TJs between endothelial cells via changes of cytoskeleton, vascular tone loss due to microtubule depolarization [49].

In our work we used 5-ALA, which is a porphyrin precursor. One of the mechanisms by which porphyrin causes PD effects is an elevation of expression of heme-transport protein (HCP1), which is capable of transporting porphyrin compounds. Recently, it has been shown that HCP1 expression is associated with increased ROS production and hypoxia that we observed in our work [50]. We suppose that PD-induced increase in oxidative stress associated with mild hypoxia and changes in TJ and adherens junction proteins might be one of mechanisms underlying PD-related BBB opening for GM1-liposomes.

4. Conclusion

Collectively, our results clearly show that application of USOCA allows to perform PD-related BBB opening non-invasively. We demonstrated that PD opened the BBB on laser dose manner and established optimal laser dose for PD-related BBB opening at 20 J/cm^2 through optical clearing skull window. Using optimal laser dose, in our *ex vivo* and *in vivo* experiments, we showed efficiency of PD to open BBB for high weight molecules (EBd albumin complex 68.5 kDa and 70kDa rhodamine-dextran) and for 100 nm GM1-liposomes that passed through the vascular endothelium, the basal membrane and distributed among astrocytes. The PD induced an increase in oxidative stress that was associated with mild hypoxia and changes in the expression of TJ (CLDN-5 and ZO-1) and adherens junction (VE-cadherin) proteins, which might be one of the mechanisms underlying PD-related BBB opening for liposomes.

These results indicate that by applying USOCA, we can realize PD-related BBB opening with low doses of photosensitizer and laser irradiation, which permits to minimize brain tissue injuries after PD. Because of its noninvasiveness, the mouse brain avoids secondary brain

Biomedical Optics EXPRESS

injuries and cortical inflammations caused by craniotomy, thus, the analysis about the mechanisms underlying PD-related BBB opening is much closer to the reality. In addition, it provides a convenient and flexible observation and light manipulation window, permitting *in vivo* observing cerebrovascular leakage with high resolution and repeated application of PD that has a great potential in glioma therapy.

Funding

National Natural Science Foundation of China (NSFC) (Grant Nos. 61860206009, 81870934, 31571002, 81701354); Foundation for Innovative Research Groups of the National Natural Science Foundation of China (Grant No. 61721092); Russian Science Foundation (17-15-01263); Fundamental Research Funds for the Central Universities, HUST (No. 2018KFYXKJC026); Director Fund of WNLO.

Acknowledgments

We also thank the Optical Bioimaging Core Facility of WNLO for support in data acquisition.

Disclosures

The authors declare that there are no conflicts of interest related to this article.

References

1. N. J. Abbott, A. A. K. Patabendige, D. E. M. Dolman, S. R. Yusof, and D. J. Begley, "Structure and function of the blood-brain barrier," Neurobiol. Dis. **37**(1), 13–25 (2010).
2. W. M. Pardridge, "Molecular Trojan horses for blood-brain barrier drug delivery," Curr. Opin. Pharmacol. **6**(5), 494–500 (2006).
3. D. Silberberg, N. P. Anand, K. Michels, and R. N. Kalaria, "Brain and other nervous system disorders across the lifespan - global challenges and opportunities," Nature **527**(7578), S151–S154 (2015).
4. M. M. Patel and B. M. Patel, "Crossing the blood-brain barrier: recent advances in drug delivery to the brain," CNS Drugs **31**(2), 109–133 (2017).
5. S. Mitragotri, "Devices for overcoming biological barriers: The use of physical forces to disrupt the barriers," Adv. Drug Deliv. Rev. **65**(1), 100–103 (2013).
6. D. S. Hersh, A. S. Wadajkar, N. Roberts, J. G. Perez, N. P. Connolly, V. Frenkel, J. A. Winkles, G. F. Woodworth, and A. J. Kim, "Evolving drug delivery strategies to overcome the blood brain barrier," Curr. Pharm. Des. **22**(9), 1177–1193 (2016).
7. V. Kiviniemi, V. Korhonen, J. Kortelainen, S. Rytky, T. Keinänen, T. Tuovinen, M. Isokangas, E. Sonkajärvi, T. Siniluoto, J. Nikkinen, S. Alahuhta, O. Tervonen, T. Turpeenniemi-Hujanen, T. Myllylä, O. Kuittinen, and J. Voipio, "Real-time monitoring of human blood-brain barrier disruption," PLoS One **12**(3), e0174072 (2017).
8. C. Poon, D. McMahon, and K. Hynynen, "Noninvasive and targeted delivery of therapeutics to the brain using focused ultrasound," Neuropharmacology **120**, 20–37 (2017).
9. P. S. Fishman and V. Frenkel, "Focused ultrasound: an emerging therapeutic modality for neurologic disease," Neurotherapeutics **14**(2), 393–404 (2017).
10. S. V. Dhuria, L. R. Hanson, and W. H. Frey 2nd, "Intranasal Delivery to the Central Nervous System: Mechanisms and Experimental Considerations," J. Pharm. Sci. **99**(4), 1654–1673 (2010).
11. I. Karaiskos, L. Galani, F. Baziaka, and H. Giamarellou, "Intraventricular and intrathecal colistin as the last therapeutic resort for the treatment of multidrug-resistant and extensively drug-resistant Acinetobacter baumannii ventriculitis and meningitis: a literature review," Int. J. Antimicrob. Agents **41**(6), 499–508 (2013).
12. J. Huppert, D. Closhen, A. Croxford, R. White, P. Kulig, E. Pietrowski, I. Bechmann, B. Becher, H. J. Luhmann, A. Waisman, and C. R. W. Kuhlmann, "Cellular mechanisms of IL-17-induced blood-brain barrier disruption," FASEB J. **24**(4), 1023–1034 (2010).
13. Z. I. Kovacs, S. Kim, N. Jikaria, F. Qureshi, B. Milo, B. K. Lewis, M. Bresler, S. R. Burks, and J. A. Frank, "Disrupting the blood-brain barrier by focused ultrasound induces sterile inflammation," Proc. Natl. Acad. Sci. U.S.A. **114**(1), E75–E84 (2017).
14. X. Dong, "Current strategies for brain drug delivery," Theranostics **8**(6), 1481–1493 (2018).
15. H. Kostron, "Photodynamic Diagnosis and Therapy and the Brain," *in Photodynamic Therapy: Methods and Protocols*, C. J. Gomer, ed. (Humana Press Inc, 2010), pp. 261–280.
16. W. Stummer, H. Stepp, O. D. Wiestler, and U. Pichlmeier, "Randomized, prospective double-blinded study comparing 3 different doses of 5-aminolevulinic acid for fluorescence-guided resections of malignant gliomas," Neurosurgery **81**(2), 230–239 (2017).
17. H. Hirschberg, F. A. Uzal, D. Chighvinadze, M. J. Zhang, Q. Peng, and S. J. Madsen, "Disruption of the blood-brain barrier following ALA-mediated photodynamic therapy," Lasers Surg. Med. **40**(8), 535–542 (2008).

Biomedical Optics EXPRESS

18. S. J. Madsen and H. Hirschberg, "Site-specific opening of the blood-brain barrier," J. Biophotonics **3**(5-6), 356–367 (2010).
19. O. Semyachkina-Glushkovskaya, J. Kurths, E. Borisova, S. Sokolovski, V. Mantareva, I. Angelov, A. Shirokov, N. Navolokin, N. Shushunova, A. Khorovodov, M. Ulanova, M. Sagatova, I. Agranivich, O. Sindeeva, A. Gekalyuk, A. Bodrova, and E. Rafailov, "Photodynamic opening of blood-brain barrier," Biomed. Opt. Express **8**(11), 5040–5048 (2017).
20. S. J. Madsen, H. M. Gach, S. J. Hong, F. A. Uzal, Q. Peng, and H. Hirschberg, "Increased nanoparticle-loaded exogenous macrophage migration into the brain following PDT-induced blood-brain barrier disruption," Lasers Surg. Med. **45**(8), 524–532 (2013).
21. H. T. Xu, F. Pan, G. Yang, and W. B. Gan, "Choice of cranial window type for in vivo imaging affects dendritic spine turnover in the cortex," Nat. Neurosci. **10**(5), 549–551 (2007).
22. J. Wang, Y. Zhang, T. H. Xu, Q. M. Luo, and D. Zhu, "An innovative transparent cranial window based on skull optical clearing," Laser Phys. Lett. **9**(6), 469–473 (2012).
23. D. Zhu, K. V. Larin, Q. Luo, and V. V. Tuchin, "Recent progress in tissue optical clearing," Laser Photonics Rev. **7**(5), 732–757 (2013).
24. J. Wang, Y. Zhang, P. C. Li, Q. M. Luo, and D. Zhu, "Review: tissue optical clearing window for blood flow monitoring," IEEE J. Sel. Top. Quant. **20**, 6801112 (2014).
25. Y. J. Zhao, T. T. Yu, C. Zhang, Z. Li, Q. M. Luo, T. H. Xu, and D. Zhu, "Skull optical clearing window for in vivo imaging of the mouse cortex at synaptic resolution:erratum," Light Sci. Appl. **7**(1), 6 (2018).
26. C. Zhang, W. Feng, Y. Zhao, T. Yu, P. Li, T. Xu, Q. Luo, and D. Zhu, "A large, switchable optical clearing skull window for cerebrovascular imaging," Theranostics **8**(10), 2696–2708 (2018).
27. S. Genheden and L. A. Eriksson, "Estimation of liposome penetration barriers of drug molecules with all-atom and coarse-grained models," J. Chem. Theory Comput. **12**(9), 4651–4661 (2016).
28. J. P. M. Jämbeck, E. S. E. Eriksson, A. Laaksonen, A. P. Lyubartsev, and L. A. Eriksson, "Molecular dynamics studies of liposomes as carriers for photosensitizing drugs: development, validation, and simulations with a coarse-grained model," J. Chem. Theory Comput. **10**(1), 5–13 (2014).
29. F. Olson, C. A. Hunt, F. C. Szoka, W. J. Vail, and D. Papahadjopoulos, "Preparation of liposomes of defined size distribution by extrusion through polycarbonate membranes," Biochim. Biophys. Acta **557**(1), 9–23 (1979).
30. M. Agrawal, D. K. Ajazuddin, D. K. Tripathi, S. Saraf, S. Saraf, S. G. Antimisiaris, S. Mourtas, M. Hammarlund-Udenaes, and A. Alexander, "Recent advancements in liposomes targeting strategies to cross blood-brain barrier (BBB) for the treatment of Alzheimer's disease," J. Control. Release **260**, 61–77 (2017).
31. Z. Belhadj, C. Zhan, M. Ying, X. Wei, C. Xie, Z. Yan, and W. Lu, "Multifunctional targeted liposomal drug delivery for efficient glioblastoma treatment," Oncotarget **8**(40), 66889–66900 (2017).
32. M. Mora, M. L. Sagristá, D. Trombetta, F. P. Bonina, A. De Pasquale, and A. Saija, "Design and characterization of liposomes containing long-chain N-acylPEs for brain delivery: Penetration of liposomes incorporating GM1 into the rat brain," Pharm. Res. **19**(10), 1430–1438 (2002).
33. L. Zhang, A. A. Habib, and D. Zhao, "Phosphatidylserine-targeted liposome for enhanced glioma-selective imaging," Oncotarget **7**(25), 38693–38706 (2016).
34. D. B. Vieira and L. F. Gamarra, "Getting into the brain: liposome-based strategies for effective drug delivery across the blood-brain barrier," Int. J. Nanomedicine **11**, 5381–5414 (2016).
35. I. A. Boldyrev, X. Zhai, M. M. Momsen, H. L. Brockman, R. E. Brown, and J. G. Molotkovsky, "New BODIPY lipid probes for fluorescence studies of membranes," J. Lipid Res. **48**(7), 1518–1532 (2007).
36. J. C. Stewart, "Colorimetric determination of phospholipids with ammonium ferrothiocyanate," Anal. Biochem. **104**(1), 10–14 (1980).
37. N. R. Kuznetsova, C. Sevrin, D. Lespineux, N. V. Bovin, E. L. Vodovozova, T. Mészáros, J. Szebeni, and C. Grandfils, "Hemocompatibility of liposomes loaded with lipophilic prodrugs of methotrexate and melphalan in the lipid bilayer," J. Control. Release **160**(2), 394–400 (2012).
38. H. L. Wang and T. W. Lai, "Optimization of Evans blue quantitation in limited rat tissue samples," Sci. Rep. **4**(1), 6588 (2015).
39. Z. Geng, X. Tong, and H. Jia, "Reactive oxygen species (ROS) mediates non-freezing cold injury of rat sciatic nerve," Int. J. Clin. Exp. Med. **8**(9), 15700–15707 (2015).
40. O. Semyachkina-Glushkovskaya, A. Pavlov, J. Kurths, E. Borisova, A. Gisbrecht, O. Sindeeva, A. Abdurashitov, A. Shirokov, N. Navolokin, E. Zinchenko, A. Gekalyuk, M. Ulanova, D. Zhu, Q. Luo, and V. Tuchin, "Optical monitoring of stress-related changes in the brain tissues and vessels associated with hemorrhagic stroke in newborn rats," Biomed. Opt. Express **6**(10), 4088–4097 (2015).
41. Z. Petrásek and P. Schwille, "Photobleaching in two-photon scanning fluorescence correlation spectroscopy," ChemPhysChem **9**(1), 147–158 (2008).
42. G. H. Patterson and D. W. Piston, "Photobleaching in two-photon excitation microscopy," Biophys. J. **78**(4), 2159–2162 (2000).
43. A. Gabizon and D. Papahadjopoulos, "Liposome formulations with prolonged circulation time in blood and enhanced uptake by tumors," Proc. Natl. Acad. Sci. U.S.A. **85**(18), 6949–6953 (1988).
44. N. Liu, X. Cui, D. M. Bryant, G. H. Glover, and A. L. Reiss, "Inferring deep-brain activity from cortical activity using functional near-infrared spectroscopy," Biomed. Opt. Express **6**(3), 1074–1089 (2015).
45. M. R. Hara, J. J. Kovacs, E. J. Whalen, S. Rajagopal, R. T. Strachan, W. Grant, A. J. Towers, B. Williams, C. M. Lam, K. Xiao, S. K. Shenoy, S. G. Gregory, S. Ahn, D. R. Duckett, and R. J. Lefkowitz, "A stress response

Biomedical Optics EXPRESS

pathway regulates DNA damage through β2-adrenoreceptors and β-arrestin-1," Nature **477**(7364), 349–353 (2011).
46. R. J. Lefkowitz and S. K. Shenoy, "Transduction of receptor signals by beta-arrestins," Science **308**(5721), 512–517 (2005).
47. P. Ballabh, A. Braun, and M. Nedergaard, "The blood-brain barrier: an overview: Structure, regulation, and clinical implications," Neurobiol. Dis. **16**(1), 1–13 (2004).
48. J. K. Hebda, H. M. Leclair, S. Azzi, C. Roussel, M. G. Scott, N. Bidère, and J. Gavard, "The C-terminus region of β-arrestin1 modulates VE-cadherin expression and endothelial cell permeability," Cell Commun. Signal. **11**(1), 37 (2013).
49. S. S. Hu, H. B. Cheng, Y. R. Zheng, R. Y. Zhang, W. Yue, and H. Zhang, "Effects of photodynamic therapy on the ultrastructure of glioma cells," Biomed. Environ. Sci. **20**(4), 269–273 (2007).
50. H. Ito and H. Matsui, "Mitochondrial reactive oxygen species and photodynamic therapy," Laser Ther. **25**(3), 193–199 (2016).